IEEE Access
Multidisciplinary | Rapid Review | Open Access Journal

SPECIAL SECTION ON RADIO FREQUENCY IDENTIFICATION AND SECURITY TECHNIQUES

Received August 22, 2018, accepted September 25, 2018, date of publication October 16, 2018, date of current version November 9, 2018.

Digital Object Identifier 10.1109/ACCESS.2018.2876286

Fabrication and Characterization of Flexible Spray-Coated Antennas

ARNO THIELENS[1,2], IGAL DECKMAN[1], REZA AMINZADEH[2], (Student Member, IEEE), ANA C. ARIAS[1], AND JAN M. RABAEY[1], (Fellow, IEEE)

[1]Berkeley Wireless Research Center, Department of Electrical Engineering and Computer Sciences, University of California at Berkeley, Berkeley, CA 94704, USA
[2]IMEC, Waves Research Group, Department of Information Technology, Ghent University, 9052 Ghent, Belgium

Corresponding author: Arno Thielens (arno.thielens@berkeley.edu)

This work was supported in part by the European Union's Horizon 2020 Research and Innovation Programme under the Marie Sklodowska-Curie with the Research Foundation Flanders (FWO).A.T. is an FWO [PEGASUS]^2 Marie Sklodowska-Curie Fellow under Grant 665501and in part by the Berkeley Wireless Research Center.

ABSTRACT This paper investigates the potential of using spray coating as a methodology for flexible antenna fabrication. The methodology has advantages compared with other antenna-printing techniques, such as screen-printing and gravure printing (more flexibility in design), or inkjet printing (faster production). The methodology is demonstrated using two different types of folded dipole antennas that are designed to operate in the ultra-high frequency radio-frequency identification (UHF RFID) band. Both antennas show good agreement between simulation and measurement of the spray-coated samples in terms of power reflection coefficient and gain. The two folded dipoles, with and without ground plane, show comparable performance in terms of gain, as similar antennas found in literature. The folded dipole on a ground plane is more stable near conductive surfaces and on the human body. Given these results, we conclude that spray coating is a good technique for printing small to medium sized batches of antennas.

INDEX TERMS Printed antennas, spray coating, radio frequency, electromagnetism.

I. INTRODUCTION

There is a growth in wireless Radio-Frequency (RF) electromagnetic (EM) applications [1], which is driven by an increased use of technologies such as wearables [2], wireless communication in vehicles [3], airplanes [4], [5], spacecrafts [6], and the internet of things [7]. These wireless technologies rely on antennas. The appropriate antenna type and fabrication method are usually determined by the particular application, frequency of operation, and scale of production under given budgetary constraints in terms of time, and resources. Some wireless technologies require relatively cheap antennas that can be produced in large volumes. One of such technologies is passive radio-frequency identification (RFID), which enables communication between a powered reader antenna and a passive, often disposable, tag antenna [8]. In passive RFID, the lifetime of an antenna is usually not expected to exceed that of the connected product or sensor.

Printed antennas are suitable for these types of applications [6], [9], [10] and have significant advantages over conventionally produced antennas. They can be produced with a small form factor in terms of volume [11], surface area [12], length [13], and mass [14], with high efficiency [15] and accuracy [16], and potentially at a low cost [17]. In particular, it is possible to print antennas that are conformal [16], flexible [18], or at least pliable [19]. These properties are desirable, in particular for passive RFID.

There are currently three main techniques for printing antennas: screen printing, gravure printing, and inkjet printing [20]. Screen printing of antennas provides a high throughput for large batches of printed antennas [21]. This fabrication method requires a screen, which covers areas on the substrate where no conductor should be deposited. During the printing process, a flood bar spreads the ink, which is later pushed through the screen by squeegee on a substrate. Once the mask is made, a large number of antenna copies can be made [22]. The production of this screen is costly and time consuming. This makes the technique not optimal for antenna prototyping. Moreover, screen printing on non-conformal objects is not trivial. Screen-printing on non-flat objects is challenging since the technique relies on a uniform gap of a few millimeters between the screen and the substrate. Gravure printing is a technique where rolls of thin substrates like glass or plastics are pressed in between two cylinders, where at least one of those is engraved with

the antennas' shape filled with conductive ink [23]. This technique can be very fast (up to several meters of print per minute). Inkjet-printing of antennas is more suitable for prototyping smaller batches of printed antennas even on non-flat substrates. The advantage of this technique is extreme flexibility in the spatial dimensions of the antenna, which can digitally be adapted from one antenna to another. However, the technique requires a mechanical translation of (a) printing nozzle(s), which takes time, in particular if multiple coatings of antenna traces are necessary. Printed antennas, and in particular printed RFID-antennas, using screen-printing [24], [25], gravure-printing [26], and inkjet-printing [19], have been demonstrated in literature. However, a general difficulty with the techniques listed above is that they all require the availability of a printer, which implies an investment cost and low flexibility in terms of the location where the antenna can be created.

Spray coating is a printing technique that might present the right balance between cost, accuracy, and flexibility on the location where the antenna can be deposited. The technique is suitable for both prototyping and the production of smaller batches of customized antennas. Additionally, the technique is an excellent precursor for a later transition towards screen printing on a larger scale. As outlined further in this manuscript, this technique requires a low-cost stencil mask and an airbrush to deposit the conductive layers, which form the antenna traces. Conductive patterns have been demonstrated using spray coating [27], but these have not been used to radiate in the RF range. The use of a low-cost stencil mask to print antennas has been demonstrated before, but only with high-end techniques such as drop-casting of silver nanowires [28]. Spray coating of antennas has been proposed in patents [29] and as a technique to coat 3D-printed structures [30], [31], but - to our knowledge- has not been demonstrated to fabricate reproducible, efficient, flexible antennas. Therefore, the goal of this manuscript is to demonstrate how a (digital) antenna design can be efficiently fabricated by a semi-automated spray-coating technique, which enables one to fabricate antennas in a reproducible and accurate manner. To this aim flexible antennas for the ultra-high frequency (UHF) RFID band are fabricated on different substrates. This manuscript will show that spray-coated antennas with good mismatch and radiation efficiency can be produced using relatively low-cost lab materials and equipment. Additionally, our goal is to investigate the on-body performance of these antennas, as wearable applications are a potential area in which the usage of these antennas would be very suitable.

II. MATERIALS AND METHODS

The following subsections provide information on the considered frequency band, the antenna design methodology, the different materials chosen to fabricate the antennas, the spray-coating methodology, and the methodology for characterizing and testing the printed antennas.

A. UHF RFID

UHF RFID is a wireless technology operated in two frequency bands 865-868 MHz and 902-928 MHz. The technology is mainly used for wireless identification of objects, but in it's latest generation of standardization allows for the transmission of sensor data as well. UHF RFID is predominantly used (or is envisioned to be used) for so-called passive sensors. These are fed energy through the RF channel and then backscatter a signal containing the requested information [32]. This manuscript will further focus on the 902-928 MHz UHF-RFID band, as this is the frequency span used in the United States.

B. ANTENNA MATERIALS

The antennas were printed on two types of flexible substrates: polyethylene-naphthalate (PEN) (Teijin DuPont Films, Chester, VA, USA) and polyimide Kapton® HPP-ST (DuPont, Wilmington, DE, USA). The thickness of the Kapton and PEN films is 125 μm and 150 μm, respectively. Kapton and PEN were used because of their well-known thermal stability (up to 400°C for Kapton and up to 150°C for PEN), electrical insulating properties, chemical stability, low surface roughness, and superior mechanical properties. It is also noteworthy that PEN is optically transparent in contrast to opaque Kapton. Thus, this choice of substrate materials covers a whole spectrum of potential printed sensors (i.e. optical, thermal and electrical) with which an antenna can be potentially integrated [33]. The printing is done with PSPI-1000 (Novacentrix, Austin TX, USA), which is a silver nanoparticles water-solvent based ink, optimized for spray coating deposition. Its sheet resistivity was characterized to be 0.3 Ω/sq./mil at 1μm dry film thickness (DFT). Improved adhesion, high conductivity, low curing temperature, and an environmentally friendly water-based solvent makes this ink promising for large scale printing. The ink's physical properties can be found in Table S.I of the Supplementary Materials. The ink's volume resistivity of 8.5 $\mu\Omega cm$ corresponds to a skin depth of 4.9 μm at 915 MHz. The antennas traces need to be thicker than this in order to minimize loss resistance [34], but cannot be too thick ($<$ 50 μm) in order to preserve flexibility. Therefore, we chose to aim at a trace thickness of 15 μm.

C. SPRAY-COATING METHODOLOGY

Figure 1 demonstrates the main stages of the antenna fabrication process. Before the fabrication stage, the antenna design was simulated using the Sim4Life software (ZMT, Zurich, Switzerland), see the next section. The antenna substrate (PEN or Kapton, in blue) was covered by Kapton®adhesive film (orange), forming a substrate/kapton stack (PEN/Kapton in Fig. 1). The antenna design was transferred to the PEN/Kapton®stack using a 30 W Universal VLS2.30 desktop laser cutter (Universal Laser Systems inc., Scottsdale, AZ, USA) after the adhesive film is placed on the substrate. The laser intensity and cutting speed were optimized to insure

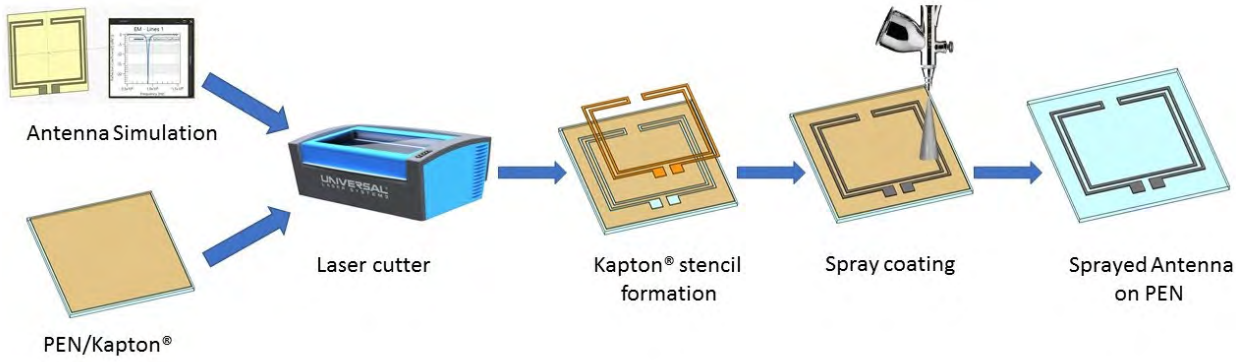

FIGURE 1. The main stages of antenna spray-coated antenna fabrication process.

cutting through the top Kapton®film only. The antenna-shaped laser-cut Kapton®film was removed, forming a Kapton®stencil on the antenna substrate. Note that this technique could be applied on other substrates as well. The PSPI-1000 ink was spray-coated using an airbrush through the stencil. The airbrush conditions (i.e. air pressure (103 kPa), ink flow, distance to substrate (20 cm) and deposition time (approx. 5 min or 20 passes)) were optimized to achieve a 15μm-thick dry film of PSPI-1000. The spray-coated antenna was annealed in vacuum oven at 120°C for 10 min to remove solvent residues and improve the conductivity of the silver traces. At the final stage the Kapton®stencil was peeled off the PEN substrate, leaving the desired antenna pattern.

D. ANTENNA DESIGN

In order to demonstrate the spray-coating fabrication technique two different dipole antennas are designed: a folded dipole and a loaded folded dipole with a ground plane. All antennas are designed to have an $S_{11} \leq -10$ dB in the 902-928 MHz band at a reference input impedance of 50 Ω.

Fig. 2 outlines the design strategy. The starting point is a printed half-wave folded dipole, which in the UHF-RFID band would have a length of approximately 16 cm. In order to reduce its size, it is possible to fold the two arms and simultaneously obtain an impedance close to 50 Ω [35]. The design parameters that were used for the dipole's optimization are shown in Figure 3. These are the dipole's width (W), the trace widths (T_1 and T_2, which are kept equal in the design without ground plane), the lengths of the different sections of the folded dipole arm (A, B, and C), and the gap (G) between both arms. We also added two pads for mounting an SMA connector with sizes (D_1 by D_2), which were kept constant at 5 mm and 4.5 mm, respectively. These parameters were optimized to obtain an $S_{11} \leq -10$ dB in the UHF-RFID frequency band. The S_{11} of a (folded) dipole will change when the antenna is placed on a conductive surface, such as the human body [36]. The usage of a conductive ground plane underneath the antenna is a common technique to isolate an antenna from underlying conductive layers and prevent this change in S_{11}.

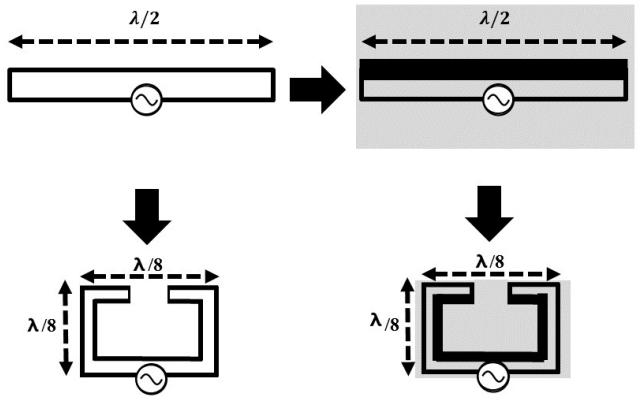

FIGURE 2. Design procedure for spray-coated (folded) dipoles. The design starts from a regular folded dipole (top left), which is bended in order to reduce the antenna surface (bottom left). In order to introduce a ground plane (gray in the top right figure), one of the widths of the antenna's strips is increased (top right). The arms are then again bended for surface reduction (bottom right). Approximate antenna dimensions are indicated by dashed double arrows.

The introduction of a ground plane underneath the antenna introduces current cancellation [37] and a reduction in impedance. However, folded dipoles' impedance can be tuned by adapting the relative difference in trace widths of both strips [35], [38]. The radiation efficiency on the other hand is expected to be reduced due to current cancellation. The parameters that need to be optimized are mainly the same, except for the trace widths, T_1 and T_2, which were in this case optimized separately.

The antennas are designed and optimized in Sim4life (ZMT, Zürich, Switzerland), which is a finite-difference time-domain electromagnetic solver. The antenna's traces are considered to be metal with a conductivity of $2x10^5$ S/m, whereas the substrate was modeled as a dielectric with properties listed in the Antenna Materials section. The antenna model is fed with an voltage source from 500 – 1500 MHz, which records the reflected voltage as a function of frequency as well. Additionally, a far-field sensor, which records the radiation pattern, and an overall field sensor, which records all fields in the simulation domain, are added to the simulations. Perfectly matched layers are applied to the edges of the simulation

domain after discretization, in order to counter unwanted reflections.

E. ANTENNA CHARACTERIZATION

An important antenna parameter is antenna Gain (G). This parameter is defined as the product of the antenna's directivity (D), the mismatch efficiency (η_{mis}), and the radiation efficiency (η_{rad}) [37]:

$$\mathbf{G} = \boldsymbol{\eta}_{\mathbf{mis}} \times \boldsymbol{\eta}_{\mathbf{rad}} \times \boldsymbol{D} = (\mathbf{1} - \mathbf{S_{11}}) \times \boldsymbol{\eta}_{\mathbf{rad}} \times \boldsymbol{D} \qquad (1)$$

with S_{11} the power reflection coefficient, defined as the ratio of the reflected power over the input power at a particular frequency [37]; and the directivity D is the ratio of the radiation intensity per unit solid angle emitted by the antenna over the same radiation intensity per unit solid angle that would be emitted by an isotropic source [37].

After the antenna fabrication, according to the models obtained in the previous subsection and using the methodology outlined above, the antennas' power reflection coefficient (S_{11}) is first measured using a vector network analyzer (Agilent N5242A, PNA-X, Santa Clara, CA, USA). The obtained S_{11} is compared to those obtained using the numerical simulations. A low S_{11} is desirable as this corresponds to a mismatch efficiency close to one (see Eq. 1). This measurement serves as a validation of the used antenna designs.

Second, we have measured the antennas' S_{11} on seven positions on the body: the left and right cheeks, the left and right pectoralis mayor, the left and right knees, and the abdomen. The S_{11} was also measured on a 76 $\times$ 76 mm^2 piece of metal. The goal of these measurements was to study the antennas' stability near conductive surfaces.

Third, we have measured the antennas' S_{11} while the antennas are bent around their middle Y and Z axes, see Fig. 3. The side with the antennas' printed traces is the convex side in these experiments. The goal of these measurements was to check whether the flexible antennas function under free-space bending conditions.

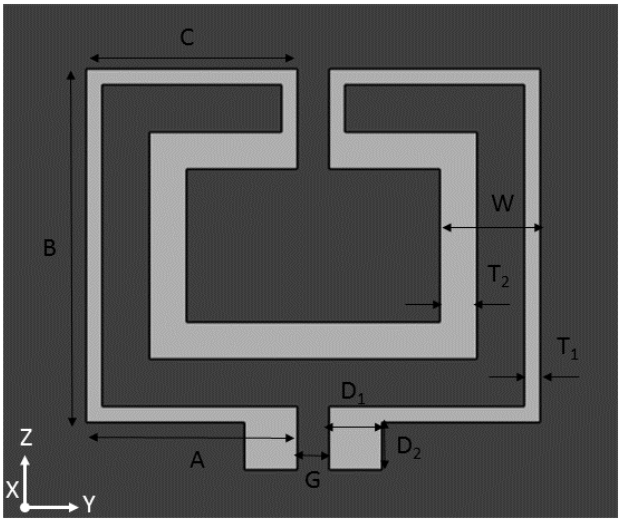

FIGURE 3. Antenna layout with design parameters.

Fourth, the antennas' Gain is measured in an anechoic chamber, using the set-up shown in Figure 4. The antennas under test are held by a Styrofoam arm and aligned to the axis of rotation of a rotational platform on one side of the chamber. On the other end of the anechoic chamber a linearly polarized standard gain horn antenna (NSI-RF-SG975, NSI-MI Technologies, Atlanta, GE, USA) with a Gain of 14 dBi is placed on the same height at a distance of 4.5 $\pm$ 0.1 m. The antenna under test and the horn antenna are connected to a VNA (ZNB20, Rohde and Schwarz, Munich, Germany) that is placed outside the chamber. This VNA is controlled using Matlab (Mathworks, Natick, MA, USA) and records all S-parameters in the two port network for 371 points in a frequency span from 750 MHz to 1.12 GHz. The VNA takes 2 frequency sweeps of the S-parameters per second. The antenna is rotated for 360° around an axis orthogonal to the chamber's floor and ceiling at a speed of 4°/s. This results in 180 frequency sweeps of the S-parameters per rotation, these can be used to determine the gain of the antenna under test as a function of rotation angle (ϕ), using:

$$S_{12}(\phi) = \left(\frac{\lambda}{4\pi d}\right)^2 \times G_{AUT}(\phi) \times G_{Horn} \qquad (2)$$

with λ the wavelength, d the distance between both antennas, G_{Horn} the Gain of the horn, and G_{AUT} the Gain of the antenna under test. This procedure is repeated for two polarizations of the horn antenna (linear polarization orthogonal to the direction of propagation and either parallel (H) or orthogonal (V) to the floor) and the antenna under test (dipole arms parallel (H) and orthogonal (V) to the floor), resulting in 4 Gain measurements per antenna under test: two copolar (VV and HH) and two crosspolar radiation patterns (VH and HV).

Finally, gain measurements using the folded dipole on a ground plane are repeated on the right pectoralis major of a human subject (28 years old, body mass index (BMI) of 23.6 kg/m^2, height 1.9 m) who took place on the rotating platform of the anechoic chamber. The subject was rotated at the same speed (4°/s) and S parameters were recorded using the VNA with the same settings. These measurements were also repeated for two polarizations (H and V) for both the horn antenna and the on-body antenna.

III. RESULTS

This section contains our results on the antenna design using numerical simulations, the antenna fabrication, the measurements and simulations of the mismatch efficiency and the Gain measurements.

A. NUMERICAL SIMULATIONS

Figure 2 shows the two studied designs: folded dipole on PEN and folded dipole on Kapton with ground plane, alongside the design parameters used in the simulations. Table 1 lists the

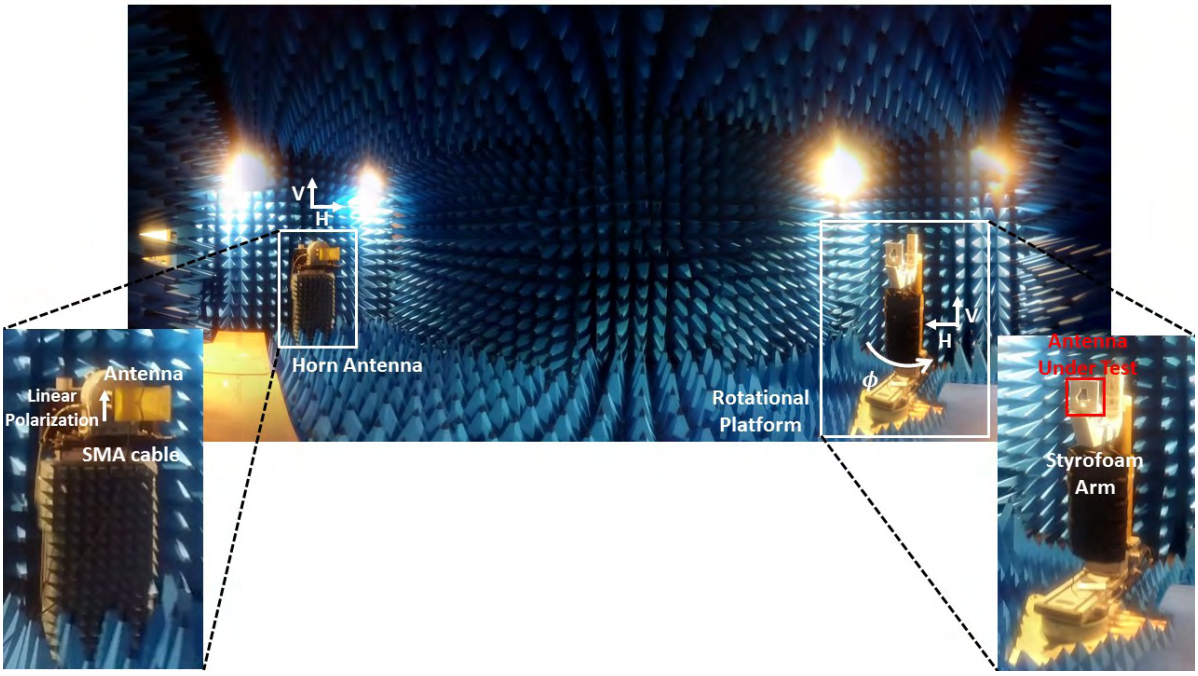

FIGURE 4. Measurement set-up in the anechoic chamber. The rotational platform with styrofoam arm used to hold the antennas under test is shown on the right, while the standard gain horn antenna is shown on the left (Horn antenna shown is not the one used in these experiments). The two studied polarizations: orthogonal to the floor and parallel to the floor and the horn's aperture, denoted by V and H, respectively, are indicated as well.

TABLE 1. Antenna dimensions (mm)[a].

	Folded Dipole	Folded Dipole on Ground Plane
A	22.5	25
B	41	40
C	21.5	24.5
D_1	5	5
D_2	4.5	4
W	3.5	15
T_1	1	1
T_2	1	8
G	3	2

a The parameters are those shown in Fig. 3

dimensions of the different parameters that result in antennas with a return loss $S_{11} \leq -10$ dB in the UHF-RFID band. Figure 5 (a) and (b) show the antennas' simulated S_{11} as a function of frequency. Following these simulations, the antennas were fabricated on their respective substrates.

Additional simulations were executed with the folded dipole on PEN with varying silver conductivity (±50%), using the same parameters listed in Table 1. These simulations showed deviations < 0.1 MHz in the S_{11} resonance peak relative to the one shown in Fig. 5 (a).

B. ANTENNA FABRICATION

Figure 6 shows microscope images of the stencil and printed silver traces on the used PEN substrate. This figure demonstrates the resolution of spray-coating techniques combined with the laser-cut stencil (see chapter Antenna Fabrication). The Kapton®stencil on the PEN substrate fabricated by laser-cutting is shown in Figure 6(a). It's important to note that the laser has a finite spot size which will increase the cut out traces, for example an input trace of 0.8 mm width results in a laser-cut line of 0.95 mm width, which corresponds to a 75 μm increase on each side. This increase should be taken into account in transferring the antenna design from the simulation software to the laser-cutter. Figure 6 (a) and (b) shows a side-by-side comparison of the used PEN substrate with the Kapton stencil (a) and the corresponding silver trace (b) after spray coating. The silver trace is confined to the area that is not shielded by the stencil. Figure 6 (c) and (d) show two adjacent traces with an intended separation of 900 μm. The measured separation is in between 890-910 μm. In general, the spray-coating deposition of PSPI-1000 results in an accuracy on the edges of the printed lines (side roughness) of ≤ 50 μm, see Figure 6 (b)-(d). This accuracy is high enough to not influence the performance of antennas with a similar scale. We verified this by executing FDTD simulations of the S_{11} of the folded dipole on PEN with trace widths of 1 mm ±0.05 mm. This variation resulted in shifts if the resonance peak of < 2.2 MHz, relative to 915 MHz. Figure 7 shows the fabricated antennas.

The antennas trace thickness was measured on 12 randomly chosen positions on six printed folded dipoles on PEN.

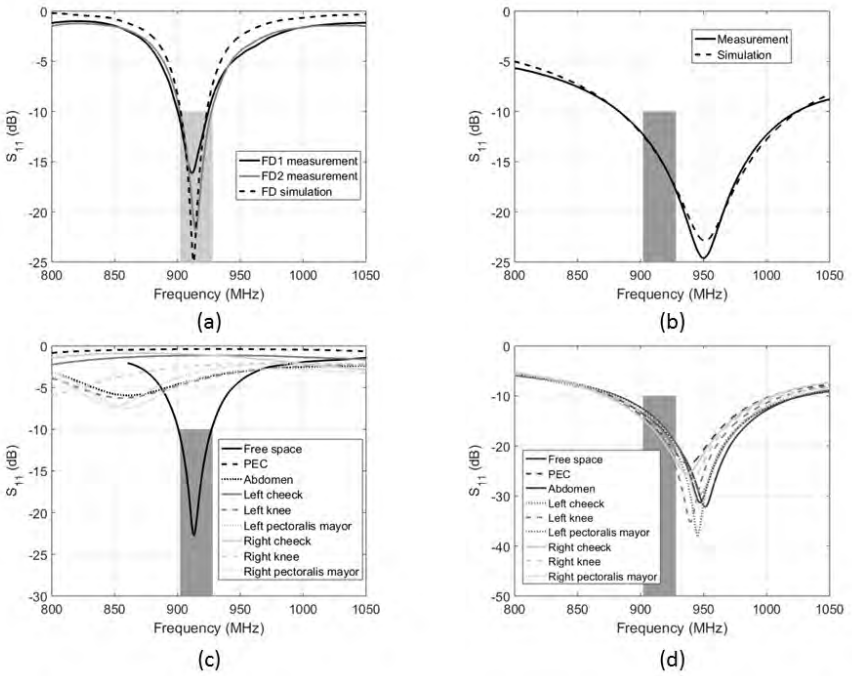

FIGURE 5. Power Reflection Coefficient (S_{11}) simulations and measurements. The grey rectangle indicates the UHF RFID band (902-928 MHz). (a) Folded dipole antenna on PEN in free space as a function of frequency. The solid lines show measurements on two printed samples (FD1 and FD2), while the dashed line shows the simulated value using the dimensions in Table 1. (b) Folded dipole on Kapton and a ground plane. The solid line shows the measurement and the dashed line shows the simulation. (c) Measurements of FD1 in free space, on 7 on-body locations, and on a metallic surface of 76 × 76 mm^2 (denoted PEC). (d) Measurements of the folded dipole on kapton and a ground plane in free space, on 7 on-body locations, and on and on a metallic surface of 76 × 76 mm^2 (denoted PEC).

The measured average trace thickness was $15 \pm 6\mu m$. The standard deviations per sample ranged from $4 - 8\mu m$, while the average thickness of each of the six measured samples ranged from 14.1 – 15.8 μm. We investigated the effect of a potential variation in trace thickness by executing FDTD simulations of the S11 of the folded dipole on PEN with trace thicknesses of 15 μm $\pm$ 6 μm. This variation resulted in small shifts if the resonance peak of $\pm$ 0.6 MHz, relative to 915 MHz.

C. RETURN LOSS

Figure 5 (a) and (b) show the simulated and measured S_{11} of the two studied dipole antennas as a function of frequency in free space. We find good agreement between simulations and measurements. The simulations of the folded dipole on PEN did not result in a configuration that spanned the full UHF RFID frequency band, so the configuration with the largest bandwidth was selected. The configuration on the ground plane allowed for more bandwidth due to the additional trace width that could be optimized. We chose to work with a configuration which has it's peak resonance higher than the frequency band of interest, since we expected a shift to lower frequencies on conductive surfaces (see Fig. 5 (d)). The S_{11} is lower than -10 dB in the complete frequency band of interest.

Figure 5 (c) and (d) show the frequency behavior of the two studied dipoles' S_{11} on the body and on a metal surface. The folded dipole without ground plane shows severe shifts in resonance frequency and absolute value of S_{11} depending on the surface underneath the dipole. These are induced by bending and the presence of the human body. The dipole on a ground plane shows smaller shifts to lower frequencies and the frequency band of interest is never out of resonance.

The folded dipole on PEN was bent around its middle Y and Z axes, see Fig. 3, for different bend radii. The bend radius is defined as the radius of the arc formed by the bent antenna. A smaller bend radius corresponds to more curvature of the antenna. The bend radii during these measurements were changed from 0.078 m until 0.022 m and 0.089 m until 0.024 m around the Y and Z axes, respectively, by increasing the antenna's curvature around the respective axes. In both bending directions, the resonance frequency of the dipole shifted slightly to higher frequencies for smaller bend radii. The largest shifts in peak resonance were found for the smallest studied bend radii: at a radius of 0.022 m around the Y axis a resonance peak of 928 MHz was found and for a curve with a radius of 0.024 m around the Z axis a resonance peak at 924 MHz was observed, respectively, in comparison to a peak resonance at 915 MHz in the antenna's flat state. The antenna's S_{11} remains < -10 dB at 915 MHz for all studied arcs around the Z axis and above a bend radius of 0.024 m around the Y axis. The antenna always has a point with $S_{11} < -10$ dB in the UHF RFID band in any of the

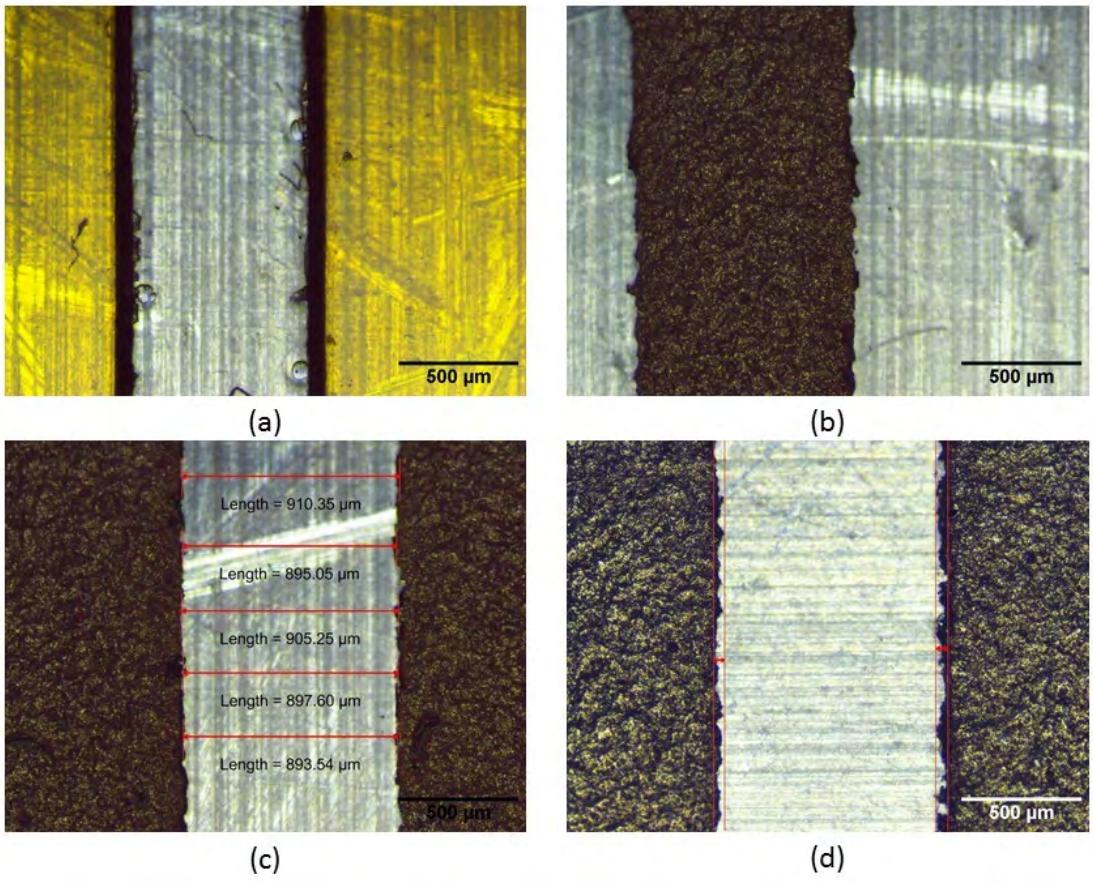

FIGURE 6. (a) Laser cut Kapton®stencil (yellow) on PEN substrate (transparent). (b)PSPI100 (dark) deposited by airbrush through the stencil. (c) two parallel PSPI100 traces of 500 μm width and an intended spacing of 900 μm, red lines indicate measurements with a microscope. (d) Shows the relative variation on the resulting traces.

studied bending conditions. The folded dipole on Kapton and a ground plane was bent with radii decreasing from 0.069 m until 0.015 m and 0.073 m until 0.023 m around the Y and Z axes, respectively. These bends did not influence the location of the peak resonance (max shift is 5 MHz). The full UHF RFID band had an $S_{11} < -10$ dB in all studied bending conditions.

D. GAIN MEASUREMENTS

Figure 8 shows four cross-sections of the folded dipole's radiation pattern in free space, using both numerical simulations and measurements in the anechoic chamber. We find very good agreement between the simulations and the measurements in terms of the shape of the radiation patterns, in particular in the co-polarized case. The maximum linear gain values are also in good agreement, see Table 2. The simulated values are higher than the measured ones, potentially due to incorrectly modeled inefficiencies. In the cross-polarized case, we find a good agreement for the VH configuration, both in terms of maximum gain and radiation pattern. The simulations of the HV configuration do not agree well with the measurements. As, Table 2 shows, this is the configuration in which the antenna has the lowest gain. Additionally, our numerical simulations show that very small errors in misalignment between the antenna's center and the Horn's center could lead to large variations in the antenna's gain pattern for this polarization setup.

Figure 9 shows the measured on-body gain of the folded dipole on Kapton and a spray-coated ground plane. All polarizations show their maximum gain in between [30°-150°], which is the angle in which the antenna, worn on the right chest, is facing the horn antenna. In the sector [210°-330°] the subject's body is in between the transmitting and receiving antenna. Therefore, the effective on-body gain is lowest in this region. Table 2 lists the measured maximum gain values for the folded dipole on a ground plane. The measured free-space Gain is lower than that of the folded dipole without ground plane. There is thus a significant loss in radiation efficiency due to current cancellation, even though the antennas impedance was tuned properly. The maximum gain reduces even further when the antennas are placed on the subject's body due to the presence of a larger conducting surface behind the antenna.

IV. DISCUSSION

Today in the field of printed electronics the most prevalent methods are screen and inkjet printing. There is a wide choice of materials, inks, screen types/cartridges and printers for

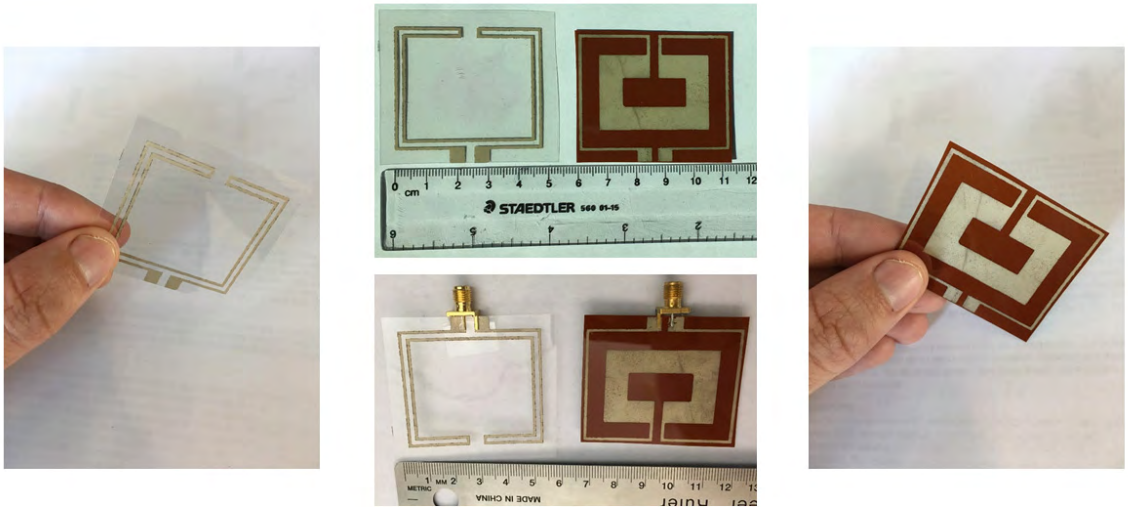

FIGURE 7. The fabricated antennas: the folded dipole on transparent PEN on the left and the folded dipole on red-brown-colored Kapton®and a ground plane on the right. The conductive traces have a grey/silver color.

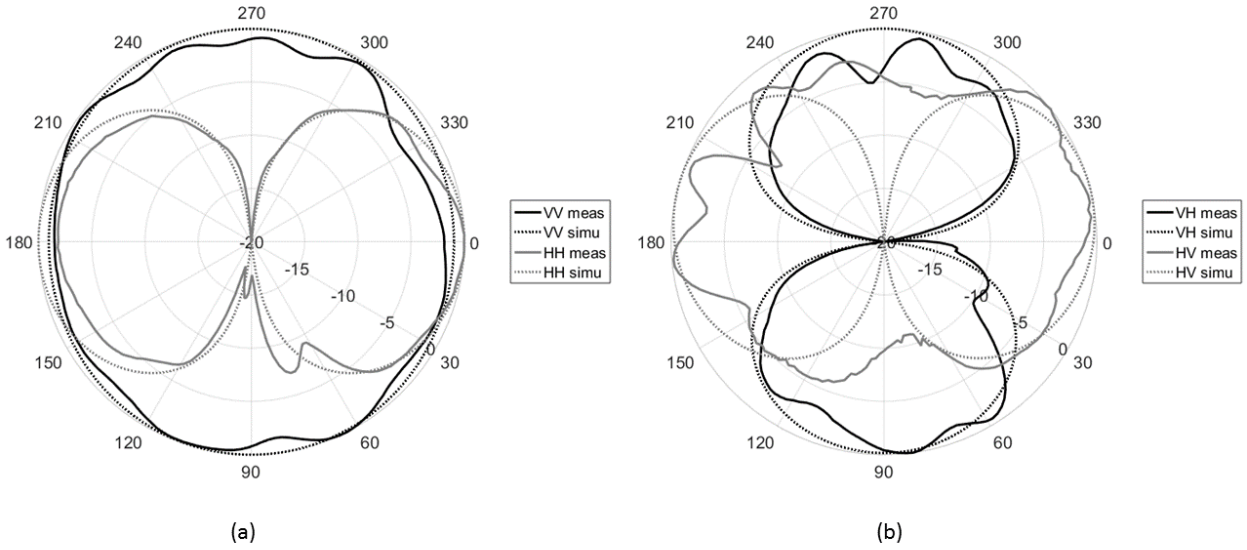

FIGURE 8. Polar plot of normalized free-space Linear Gain of the folded dipole antenna on PEN. The azimuth angle shows the angle of rotation of the antenna under test, while the radial dimension is the normalized Linear Gain (in dB). 0° indicated the azimuth angle where the plane in which the dipole is printed is parallel to the aperture of the horn, with the printed side facing away from the horn. Each curve has been renormalized to its own maximum, listed in Table2. The normalized gain values in are shown for four different sets of linear polarizations: VV, HH, VH, and HV, where the first letter indicates the horn's polarization and the second the dipole's polarization, respectively. (a) Measurements with co-polarized dipole and horn antenna. (b) Measurement with cross-polarized dipole and horn antenna.

both methods. Both methods allow to achieve high resolution of prints with line width of 20-40 μm [39]. The three main differences between these methods are: modifiability of the print design, printing time and thickness of deposited layers. Inkjet printing allows easy modification of design but, printing speed and thickness of deposited layer (300 nm) are much lower in compare to screen printing. The screen printing is high speed printing technique suitable for roll-to-roll (R2R) fabrication and characterized by high thickness (10-15μm) of the deposited layers but any modification of print design requires fabrication of a new screen. Both methods are limited to 2D small area prints (width 0.5m). Another printing method that gets more and more popular these days is spray coating. This method allows large area printing of electronic devices on 2D and 3D surfaces. The deposition thickness can be controlled by deposition conditions and number of deposited layers. Spray coating can be applied manually (e.g. airbrush) in combination with stencil or by 3 or 5 axis printers (e.g. optomec, neotech-amt) for high resolution prints. Both techniques allow easy modification of print design. Spray coating can replace inkjet and screen printing at research and development stage of a project when print design changes often and high throughput is not required. Figure 6 demonstrates that the technique

TABLE 2. Maximum Gain[a] (dBI) of both antennas: folded dipole on PEN and folded dipole on Kapton and ground plane.

Linear Gain (dBi)	VV	HH	VH	HV
Folded Dipole in Free Space				
Measured	0.8	0.3	-3.3.	-8.7
Simulated	1.3	0.3	-2.5	-40
Folded Dipole on Ground Plane				
Measured, free space	-8.2	-9.4	-8.2	-7.4
Measured, on body	-14	-14	-11	-9.8

a The gain values in dBi are shown for four different sets of polarizations: VV, HH, VH, and HV, where the first letter indicated the horn's polarization and the second the dipole's polarization, respectively. Measured and Simulated gain values in free space are shown for the dipole on PEN, while measured free-space and on-body values are shown for the dipole on a ground plane.

provides enough resolution ($\leq$50 μm) for antennas in the UHF RFID band, while Figure 7 shows that it is possible to use this technique to transfer a digital antenna design on plastic substrates. Two types of antennas were fabricated using this method: a folded dipole on PEN and a folded dipole on Kapton with ground plane.

The gain and impedance of the folded dipole on PEN studied in this manuscript correspond very well to a similar design presented in [35] on a rigid surface. They observe a slightly higher maximal gain, 1.2 dBi simulated and 1.8 dBi measured, than the dipole investigated in this manuscript, 1.3 dBi simulated and 0.8 dBi measured. However, the bandwidth in this manuscript, 22 MHz simulated and 23 MHz measured, is larger than the one obtained in [35], 8 MHz measured and simulated.

We observed a reduced gain for the folded dipole on the ground plane, which is in line with what has been observed for other metal mounted RFID antennas [40]. The maximum gain for a surface of 44 $\times$ 44 mm^2 is 0.1 dBi 40. UHF-RFID antennas were fabricated on Kapton with the same thickness and a similar surface (90 $\times$ 20 mm^2) in [42] and showed an effective gain between $-$22 dBi and $-$14 dBi on the body of human subjects and a tissue simulating phantom. The effective gain of printed antennas on a ground plane can be improved by increasing the antenna's volume [40]. An effective approach would to increase the antenna's thickness. A UHF-RFID antenna of 72 $\times$ 26 $\times$ 3 mm^3 with a Gain of 0 dBi is presented in [43]. A UHF-RFID antenna which tries to find a balance between volume (62 $\times$ 32 $\times$ 0.79 mm^3) and gain ($-$7 dBi) is presented in [8]. These antennas have thicknesses of approximately 25 and 6 times, respectively, the substrate thickness used in this manuscript. Increasing volume potentially increases the mass and cost of the antennas, while also decreasing the flexibility and general wearability. The right balance between volume, gain, and antenna bandwidth will always depend on the envisioned application.

V. STRENGTHS, LIMITATIONS, AND FUTURE RESEARCH

The antenna fabrication methodology presented in this paper has several strengths. First, the necessary materials are common or relatively easy to obtain. Second, the usage of plastic stencils is inexpensive, provides flexibility in antenna design, and can be accurate enough for the fabrication of antennas. Third, the antennas can be applied on a variety of substrates. In comparison to screen printing, the proposed technique allows for faster, easier, and cheaper modification of antenna designs and ensures contact between the stencil and the substrate by design. In comparison to inkjet printing, the technique allows faster deposition of thicker layers, can be used on larger areas, and curved substrates.

The fabricated antennas are lightweight, efficient, and when used on a ground plane are relatively stable on the body while maintaining an on-body gain that is comparable to what is shown in literature for similar dimensions. This makes the antennas very suitable for usage in wearable applications such as wireless body area networks. The spray-coating method is limited to smaller batches of antennas, since it requires manually spraying the antenna. However, it could also be automated to achieve high throughput. Spray-coating can results in low-conductivity traces when not enough layers of paint or ink are applied, which degrades antenna performance. The method relies on the accuracy of the stencil, which is also the case for other printing techniques such as stencil-blade coating, screen printing, gravure printing. The fabricated antennas are flexible and can conform to different surfaces. However, they cannot be stretched, nor is their efficiency guaranteed under all bending radii. Finally, a higher (on-body) gain could be achieved if the antennas are printed on higher-volume substrates. In our future research, we will focus on integrating these antennas with other printed components to work towards all-printed wireless systems or so-called hybrid wireless systems that combine printed traces with surface mount components. Additionally, we will experiment with different antenna designs using the same printing

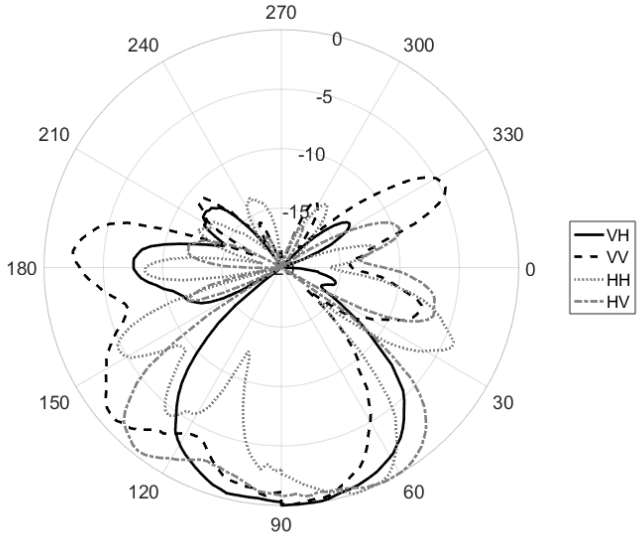

FIGURE 9. Polar plot of normalized on-body Gain of the folded dipole antenna on Kapton and a ground plane. The azimuth angle shows the angle of rotation of the antenna under test, while the radial dimension is the normalized Gain (in dB). 0° indicated the azimuth angle where the subject was facing away from the horn antenna. Each curve has been renormalized to its own maximum, listed in Table 2. The normalized gain values in are shown for four different sets of polarizations: VV, HH, VH, and HV, where the first letter indicates the horn's polarization and the second the dipole's polarization, respectively.

technique and perform a more in-depth analysis of different printing techniques for the same antenna design and materials.

VI. CONCLUSIONS

In this paper we propose and investigate a method for spray coating antennas. The methodology has advantages over the current state of the art in printed antennas in terms of flexibility in design and production time for small to medium sized numbers of antennas. The methodology is demonstrated by fabricating two types of folded dipole antennas in the UHF RFID band: one with and one without a ground plane on two different flexible, plastic substrates. We find a good agreement between the simulated antennas power reflection coefficient and Gain, two important antenna parameters. The folded dipole without a ground plane has a free-space radiation efficiency and gain comparable to similar antennas demonstrated in literature. The antenna with a ground plane has a stable power reflection coefficient on conductive surfaces and a gain that is comparable to antennas with similar sizes on ground planes. These results show that the proposed methodology is suitable for fast and accurate fabrication of planar antennas.

REFERENCES

[1] P. Cerwall, "Ericsson mobility report 2017," Ericsson, Stockholm, Sweden, White Paper, 2017.
[2] J. M. Rabaey, "The human intranet—Where swarms and humans meet," in *Proc. DATE*, Mar. 2015, pp. 637–640.
[3] D. Zamberlan, "Convergence in automotive and wireless technologies: Updates on perspectives for vehicular antennas," in *Proc. IEEE-APS Top. Conf. Antennas Propag. Wireless Commun. (APWC)*, Sep. 2017, pp. 320–323.
[4] N. L. Armstrong and Y. M. M. Antar, "Investigation of the electromagnetic interference threat posed by a wireless network inside a passenger aircraft," *IEEE Trans. Electromagn. Compat.*, vol. 50, no. 2, pp. 277–284, May 2008.
[5] Z. Li *et al.*, "Capacity and spatial correlation measurements for wideband distributed MIMO channel in aircraft cabin environment," in *Proc. IEEE WCNC*, Apr. 2012, pp. 1175–1179.
[6] R. Waterhouse, *Printed Antennas for Wireless Communications*. Amsterdam, The Netherlands: Elsevier, 2007.
[7] L. Atzori, A. Iera, and G. Morabito, "The Internet of Things: A survey," *Comput. Netw.*, vol. 54, no. 15, pp. 2787–2805, Oct. 2010.
[8] T. Björninen and F. Yang, "Signal strength readout and miniaturised antenna for metal-mountable UHF RFID threshold temperature sensor tag," *Electron. Lett.*, vol. 51, no. 22, pp. 1734–1736, Oct. 2015.
[9] K. V. S. Rao, P. V. Nikitin, and S. F. Lam, "Antenna design for UHF RFID tags: A review and a practical application," *IEEE Trans. Antennas Propag.*, vol. 53, no. 12, pp. 3870–3876, Dec. 2005.
[10] C. Reig and E. Ávila-Navarro, "Printed antennas for sensor applications: A review," *IEEE Sensors J.*, vol. 14, no. 8, pp. 2406–2418, Aug. 2014.
[11] C. M. Kruesi, R. J. Vyas, and M. M. Tentzeris, "Design and development of a novel 3-D cubic antenna for wireless sensor networks (WSNs) and RFID applications," *IEEE Trans. Antennas Propag.*, vol. 57, no. 10, pp. 3293–3299, Oct. 2009.
[12] A. A. Babar *et al.*, "Inkjet-printable UHF RFID tag antenna on a flexible ceramic- polymer composite substrate," in *IEEE/MTT-S Int. Microw. Symp. Dig.*, Jun. 2012, pp. 1–3.
[13] H. Liu, S. Ishikawa, A. An, S. Kurachi, and T. Yoshimasu, "Miniaturized microstrip meander-line antenna with very high-permittivity substrate for sensor applications," *Microw. Opt. Technol. Lett.*, vol. 49, no. 10, pp. 2438–2440, 2007.
[14] J.-M. F. Gonzalez, P. Padilla, J. F. Valenzuela-Valdes, J.-L. Padilla, and M. Sierra-Perez, "An embedded lightweight folded printed quadrifilar helix antenna: Uav telemetry and remote control systems," *IEEE Antennas Propag. Mag.*, vol. 59, no. 3, pp. 69–76, Jun. 2017.
[15] O. Kramer, T. Djerafi, and K. Wu, "Vertically multilayer-stacked Yagi antenna with single and dual polarizations," *IEEE Trans. Antennas Propag.*, vol. 58, no. 4, pp. 1022–1030, Apr. 2010.
[16] J. J. Adams *et al.*, "Conformal printing of electrically small antennas on three-dimensional surfaces," *Adv. Mater.*, vol. 23, no. 11, pp. 1335–1340, Mar. 2011.
[17] V. Subramanian *et al.*, "Progress toward development of all-printed RFID tags: Materials, processes, and devices," *Proc. IEEE*, vol. 93, no. 7, pp. 1330–1338, Jul. 2005.
[18] S.-D. Jang and J. Kim, "Passive wireless structural health monitoring sensor made with a flexible planar dipole antenna," *Smart Mater. Struct.*, vol. 21, no. 2, p. 027001, 2012.
[19] R. Vyas *et al.*, "Inkjet printed, self powered, wireless sensors for environmental, gas, and authentication-based sensing," *IEEE Sensors J.*, vol. 11, no. 12, pp. 3139–3152, Dec. 2011.
[20] D. Godlinski, R. Zichner, V. Zöllmer, and R. R. Baumann, "Printing technologies for the manufacturing of passive microwave components: Antennas," *IET Microw. Antennas Propag.*, vol. 11, no. 14, pp. 2010–2015, Nov. 2017.
[21] R. Zichner and R. Baumann, "Roll-to-roll screen printed radio frequency identification transponder antennas for vehicle tracking systems," *Jpn. J. Appl. Phys.*, vol. 52, no. 5S1, p. 05DC24, 2012.
[22] A. E. Ostfeld, I. Deckman, A. M. Gaikwad, C. M. Lochner, and A. C. Arias, "Screen printed passive components for flexible power electronics," *Sci. Rep.*, vol. 5, Oct. 2015, Art. no. 15959.
[23] M. Pudas, N. Halonen, P. Granat, and J. Vähäkangas, "Gravure printing of conductive particulate polymer inks on flexible substrates," *Prog. Organic Coat.*, vol. 54, no. 4, pp. 310–316, 2005.
[24] Y. Kim, B. Lee, S. Yang, I. Byun, I. Jeong, and S. M. Cho, "Use of copper ink for fabricating conductive electrodes and RFID antenna tags by screen printing," *Current Appl. Phys.*, vol. 12, no. 2, pp. 473–478, 2012.
[25] D.-Y. Shin, Y. Lee, and C. H. Kim, "Performance characterization of screen printed radio frequency identification antennas with silver nanopaste," *Thin Solid Films*, vol. 517, pp. 6112–6118, Sep. 2009.
[26] H. Zhu *et al.*, "A gravure printed antenna on shape-stable transparent nanopaper," *Nanoscale*, vol. 6, no. 15, pp. 9110–9115, 2014.
[27] Y. Zheng, S. Li, W. Shi, and J. Yu, "Spray-coated nanoscale conductive patterns based on *in situ* sintered silver nanoparticle inks," *Nanosc. Res. Lett.*, vol. 9, p. 145, Mar. 2014.

[28] L. Song, A. C. Myers, J. J. Adams, and Y. Zhu, "Stretchable and reversibly deformable radio frequency antennas based on silver nanowires," *ACS Appl. Mater. Interfaces*, vol. 6, no. 6, pp. 4248–4253, 2014.
[29] H. Kogure, Y. Akaki, and S. Nakamura, "Method for forming automotive antenna," U.S. Patent 0 263 405 A1, Dec. 30, 2004.
[30] S. Lee, G. Jeoung, and J. Choi, "Three-dimensional-printed tapered cavity-backed flush-mountable wideband antenna for UAV," *Microw. Opt. Technol. Lett.*, vol. 59, no. 12, pp. 2975–2981, 2017.
[31] J. Tak, D.-G. Kang, and J. Choi, "A lightweight waveguide horn antenna made via 3D printing and conductive spray coating," *Microw. Opt. Technol. Lett.*, vol. 59, pp. 727–729, Mar. 2017.
[32] J. Zhang, G. Y. Tian, A. M. J. Marindra, A. I. Sunny, and A. B. Zhao, "A review of passive RFID tag antenna-based sensors and systems for structural health monitoring applications," *Sensors*, vol. 17, no. 2, pp. 9110–9115, 2017.
[33] Y. Khan, A. E. Ostfeld, C. M. Lochner, A. Pierre, and A. C. Arias, "Monitoring of vital signs with flexible and wearable medical devices," *Adv. Mater.*, vol. 28, pp. 4373–4395, 2016.
[34] D. D. Deavours, K. Demarest, A. Syed, D. D. Deavours, K. Demarest, and A. Syed, "Effects of antenna material on the performance of UHF RFID tags," in *Proc. IEEE Int. Conf. RFID*, Grapevine, TX, USA, Mar. 2007, pp. 57–62.
[35] Y. T. Im, J. H. Kim, and W. S. Park, "Matching techniques for miniaturized UHF RFID loop antennas," *IEEE Antennas Wireless Propag. Lett.*, vol. 8, pp. 266–270, 2009.
[36] R. Aminzadeh *et al.*, "On-body calibration and measurements using personal radiofrequency exposimeters in indoor diffuse and specular environments," *Bioelectromagnetics*, vol. 37, no. 5, pp. 298–309, 2016.
[37] C. A. Balanis, *Antenna Theory: Analysis and Design*. Hoboken, NJ, USA: Wiley, 2005.
[38] R. Lampe, "Design formulas for an asymmetric coplanar strip folded dipole," *IEEE Trans. Antennas Propag.*, vol. AP-33, no. 9, pp. 1028–1031, Sep. 1985.
[39] W. J. Hyun, E. B. Secor, M. C. Hersam, C. D. Frisbie, and L. F. Francis, "High-resolution patterning of graphene by screen printing with a silicon stencil for highly flexible printed electronics," *Adv. Mater.*, vol. 27, no. 1, pp. 109–115, 2015.
[40] T. Björninen, L. Sydänheimo, L. Ukkonen, and Y. Rahmat-Samii, "Advances in antenna designs for UHF RFID tags mountable on conductive items," *IEEE Antennas Propag. Mag.*, vol. 56, no. 1, pp. 79–103, Feb. 2014.
[41] R. F. Harrington, "Effect of antenna size on gain, bandwidth, and efficiency," *J. Res. Nat. Bureau Standards*, vol. 64D, no. 1, pp. 1–12, Jan./Feb. 1960.
[42] K. Koski, T. Björninen, L. Sydänheimo, L. Ukkonen, and Y. Rahmat-Samii, "A new approach and analysis of modeling the human body in RFID-enabled body-centric wireless systems," *Int. J. Antennas Propag.*, vol. 2014, Mar. 2014, Art. no. 368090.
[43] H.-W. Son and S.-H. Jeong, "Wideband RFID tag antenna for metallic surfaces using proximity-coupled feed," *IEEE Antennas Wireless Propag. Lett.*, vol. 10, pp. 377–380, 2011.

ARNO THIELENS received the M.Sc. degree in engineering (applied physics) from Ghent University in 2010, and the Ph.D. degree in applied physics from Ghent University, in 2015. His research focused on personal exposure assessment to radio-frequency electromagnetic fields and numerical dosimetry.

Since 2015, he has been a Post-Doctoral Researcher with Waves (Information Technology Department). He was a Post-Doctoral Fellow of the Institute for Science and Innovation, Flanders, Belgium, from 2016 to 2017. In 2017, he joined the Berkeley Wireless Research Center, University of California at Berkeley, Berkeley, where he is involved in the development of the human intranet. He also received an Honorary Fellowship by the Belgian American Education Foundation in 2017.

Dr. Thielens was a recipient of the Joseph James Morrissey Memorial Award issued by the Bioelectromagnetics Society and the European Bio Electromagnetics Association in 2013. He also received the 2015 International Union of Radio Science [Union Radio-Scientifique Internationale or (URSI)] Young Scientist Award.

IGAL DECKMAN received the B.Sc. degrees in chemistry in materials engineering from Technion–Israel Institute of Technology and the Ph.D. degree from the Technion–Israel Institute of Technology, in 2014.

He was a Post-Doctoral Fellow with the Department of Electrical Engineering and Computer Sciences, University of California at Berkeley, Berkeley, from 2014 to 2018. He conducted research on fully printed optoelectronic devices, flexible antennas, and RF devices. He is currently a New Technology Engineer with Analog Devices, Inc.

REZA AMINZADEH (S'10) received the M.Sc. degree in electrical engineering from the Sharif University of Technology, Iran, in 2014. He is currently pursuing the Ph.D. degree in wireless body area networks for the characterization of human exposure to radio-frequency electromagnetic fields with the Department of Information Technology, Ghent University, Belgium. From 2012 to 2014, he was a Researcher with the Computational Electromagnetics Lab, Sharif University of Technology, where he conducted research on numerical and experimental assessment of millimeter-wave reflectometry for detection of skin cancer. He was served as member of the technical program committee for the 14th, 15th, and 17th National Iranian Student Conference on Electrical Engineering from 2011 to 2014. He has authored or co-authored of about 24 peer-reviewed scientific journals and conference papers in bioelectromagnetics. He was a recipient of the third Best Platform Presentation and Scientific Paper Award in BioEM2018, the Joint Meeting of The Bioelectromagnetics Society and the European BioElectromagnetics Association. His research interests include numerical and experimental dosimetry, measurement and theoretical modeling of dielectric properties of biological tissues, and the development of tissue-equivalent phantoms for mm-wave band, including the 5G technology and on/in body radio wave propagation.

ANA C. ARIAS received the bachelor's and master's degrees from the Federal University of Paraná in Curitiba, Brazil, in 1997 and 1995, respectively, and the Ph.D. degree from the University of Cambridge, U.K., in 2001, all in physics. She joined the University of California at Berkeley, Berkeley, in 2011.

She was the Manager of the Printed Electronic Devices Area and a member of Research Staff at PARC, a Xerox Company. She went to PARC, in 2003, from Plastic Logic in Cambridge, U.K., where she led the semiconductor group. Her research focuses on the use of electronic materials processed from solution in flexible electronic systems. She uses printing techniques to fabricate flexible large area electronic devices and sensors.

JAN M. RABAEY was a Research Manager with imec from 1985 to 1987. He has served as the Electrical Engineering Division Chair at Berkeley. He currently holds the Donald O. Pederson Distinguished Professorship at the University of California at Berkeley. He is also the Founding Director of the Berkeley Wireless Research Center and the Berkeley Ubiquitous Swarm Lab.

He has made high-impact contributions to a number of fields, including advanced wireless systems, low power integrated circuits, mobile devices, sensor networks, and ubiquitous computing. His current interests include the conception of the next-generation distributed systems, and the exploration of the interaction between the cyber and the biological world.

He has been involved in a broad variety of start-up ventures, including Cortera Neurotechnologies, where he is currently a Co-Founder. He is a member of the Royal Flemish Academy of Sciences and Arts of Belgium. He is a recipient of major awards, amongst which the IEEE Mac Van Valkenburg Award, the European Design Automation Association Lifetime Achievement Award, the Semiconductor Industry Association University Researcher Award, and the SRC Aristotle Award. He has received honorary doctorates from Lund (Sweden), Antwerp (Belgium), and Tampere (Finland).